Escola de Primavera de Transição e Turbulência
Blumenau 2022

ABCM
13th Spring School on Transition and Turbulence
September 19th-23rd, 2022, Blumenau, SC, Brazil

EPTT-2022-0044
FEATURES OF MIXING TRANSITION IN 2D MIXING LAYERS SIMULATED WITH HIGH ORDER SPECTRAL/HP METHODS

Daniel Garcia-Ribeiro
Rodrigo José Albuquerque Barreira
Vinicius Malatesta
Rodrigo C. Moura
Instituto Tecnológico de Aeronáutica (ITA), São José dos Campos, São Paulo, Brazil
danieldgr@ita.br

Abstract. *Turbulent flows are a major topic of research because they have plenty of different applications, besides there is still much to understand about them. In this context, mixing layers arise as a specific kind of flow that can reach turbulence under high enough Reynolds number as it is in other types of flow. Also, specifically for mixing layers, the Reynolds number of the flow increases with the downstream direction, which permits the visualization of the turbulence development and, before that, the so-called mixing transition phenomenon. Although mixing layers have been extensively studied in the past and the mixing transition has already been documented, the literature relies majority on experimental investigations or on 3D numerical simulations. Therefore, this paper analyses a 2D mixing layer and reports features of mixing transition. To this end, an open-source spectral/hp element method software with the Continuous Galerkin scheme, namely Nektar++, is used to resolve and capture the small scales associated with the mixing transition.*

Keywords: *Mixing layer, Mixing transition, iLES, Continuous Galerkin method, High order spectral/hp methods*

1. INTRODUCTION

Turbulent flows are a topic of great interest of academia and industrial communities due to their natural complex behaviors - in part still not explained - and many applications in different industries as the aeronautical one. For instance, some aspects related to non-homogeneous isotropic turbulence and wall turbulence need more clarification, and turbulent jets are a common feature of aircraft and rockets (Pope, 2000). In this vast context of turbulent flows, this paper focus on studying the specific phenomenon of mixing transition that occurs in shear layers, jets and also in other types of flows (Dimotakis, 2000). First of all, we need to present some general aspects of turbulent flows simulations before deepening in the mixing transition itself.

The study of fluid dynamic problems starts with the definition and simplification of the Navier-Stokes and energy balance equation. There are specific occasions that these equations have analytic solutions, however the great majority of flows do not have that kind of solutions. Therefore, researchers and engineers have to rely upon experimental tests or numerical methods, these last ones being approximations of the partial derivatives by algebraic expressions or projections of the conserved parameters into polynomial spaces. Examples of these approaches would be the so-called finite difference method, which uses Taylor's series, and the spectral/*hp* element method. There are other methods in the literature, but all of them will turn the fluid dynamic equations into tractable equations by the computers.

Another issue is the turbulent behavior that a flow may present under specific conditions as high Reynolds number, *Re*. In a short description, turbulence is a 3D-phenomenon characterized by the presence of eddies, the chaotic behavior of the solution and the random description of the flow information. Towards numerically treating turbulence, there are specific numerical approaches as the Direct Numerical Simulation (DNS), Large Eddy Simulation (LES) and (Unsteady) Reynolds-Averaged Navier-Stokes equation (U-RANS). Basically, the DNS approach solves completely the Navier-Stokes equations, i.e., it solves for the full time and length scales range of turbulence, and is considered the most reliable approach. As for the RANS approach, which is the one most commonly used method by industry, it computes only the average values of the flow information and uses specific closure models to compute the unknown term of the averaged equation – which is the Reynolds stress tensor. This average process leads to a much lower computational cost of the equations, being that the main reason of its wide usage. The LES approach applies a filter to filter out the smallest turbulence scales, lying somewhere between the DNS and RANS methods in terms of accuracy and computational cost. An alternative to LES is the implicit LES (iLES) or also called under-resolved DNS, which do not apply a specific filter, relying just on the numerical dissipation of the method (Pope, 2000; Silveira Neto, 2020).

Basically, mixing layers are a kind of flow where a layer of a fluid flows over another one with a relative speed (see Fig. 1). As the *Re* increases, the flow passes through a transitional range, i.e. it starts to transition from a laminar state to a turbulent one, until a certain *Re* where the flow is fully turbulent. We reinforce the idea that this transitional range may vary depending on initial and boundary conditions and that turbulent flows are not sustainable if the *Re* is below a critical value (Pope, 2000).

As will be shown later in Sec. 2, the *Re* of a mixing layer increases linearly with the stream-wise coordinate, having,

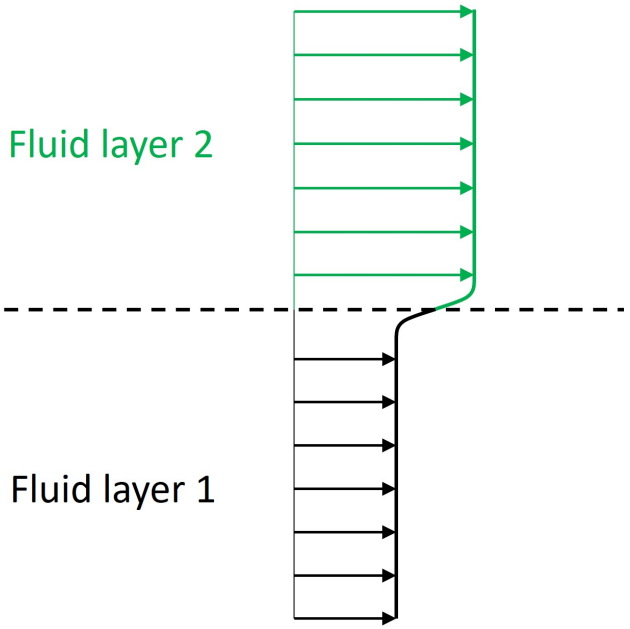

Figure 1: Representation of a generic mixing layer velocity profile. Fluid layer 2 flows over fluid layer 1 with a higher velocity magnitude.

thus, a local attribute. This fact makes spatial mixing layers interesting to study because one can see the development of a laminar flow into a fully-turbulent one as the *Re* increases and also can note the increase of mixing between the species. In addition, it has been noted that, besides the large-scale coherent structures that dominate the flow and are seen until high *Re*, the stream-wise vortices becomes part of the energy cascade process to the small scale through the vortex stretching mechanism. Above a certain value of a Reynolds number, the stream-wise structures become unstable, which is associated with a fast increase in the molecular mixing, whereas the development of the great eddies is not effect. This process of increasing mixing is known as mixing transition (Papamoschou and Gharib, 2020; Dimotakis, 2000; Koochesfahani and Dimotakis, 1986; Brown and Roshko, 1974). To illustrate this phenomenon, Fig. 2 presents shadow-graph motion pictures of a mixing layer experiment. One can observe that the coherent structures persist with the increase of the *Re* and that much smaller scales appears with a relatively small increase in the Reynolds number.

This paper aims at identifying features of the mixing transition in a 2D mixing layer using a numerical approach based on a spectral/*hp* element method, namely Continuous Galerkin (CG) method. To this end, this manuscript is organized as follows: an introduction to theme of mixing transition and numerical simulations of turbulent flows is presented in Sec. 1. The numerical method, along with the simulation setup parameters, and the analysis methodology of the mixing layer are introduced in Sec. 2. The results and all related discussions are argued in Sec. 3. Finally, the main conclusions of this study as well future perspective of research are presented in Sec. 4.

2. MATERIALS AND METHODS

This section introduces the numerical approach used for formulating the aimed analysis. Therefore, the utilized equations, the numerical discretization, the boundary and initial conditions and others setup parameters are described herein.

2.1 Numerical approach

This study uses the under-resolved DNS approach to resolve the flow field of the hereafter described mixing layer. As briefly described in Sec. 1, that method relies upon the numerical dissipation implicit within the numerical method to model the dissipation of the turbulence smallest length-scales. For the problem under consideration, the body force-free flow is composed by a Newtonian fluid, and its properties are considered constant and isotropic. Therefore, the continuity and momentum equations solved in the simulations are:

$$\nabla \cdot \mathbf{U} = 0 \tag{1}$$

$$\rho \frac{D\mathbf{U}}{Dt} = \mu \nabla^2 \mathbf{U} - \nabla P \tag{2}$$

Where U is the velocity vector, ρ and μ are the fluid density and molecular (dynamic) viscosity and P is the pressure.

The CG method is based on Galerkin projection of functions in order to solve partial differential equations (PDE). Basically, having a PDE, which is represented by an operator $\mathcal{R}$ applied to some information as in $\mathcal{R}(u) = 0$, the

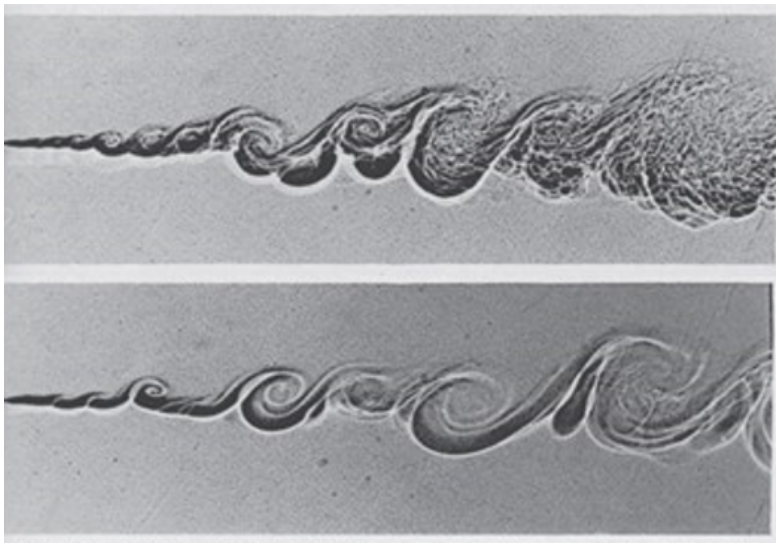

Figure 2: Effect of Reynolds number on a mixing layer of two species with the same dynamic pressure. (top) *Re* is proportional to 4×10 (pressure = 4 atm, U_1 = 10 m/s); (bottom) 2×10. Reproduced from Brown and Roshko (1974).

Galerkin method's first step is to apply the Galerkin projection on the exact solution of the PDE to approximate it as stated in Eq. 3.

$$u^{\delta}(x) = \sum_{j=0}^{P} \hat{u}_j \phi_j(x) \tag{3}$$

In this previous equation, $u^{\delta}(x)$ is the projection of the exact solution ($u(x)$), $\hat{u}_j$ is a set of coefficients from the projection and $\phi_j(x)$ is a set of basis functions that form a polynomial space $\mathcal{S}_P$ of order P. Then, the second step requires that the projection of $\mathcal{R}(u^{\delta})$ onto $\mathcal{S}_P$ to be zero as follows:

$$\int \mathbf{\Phi}(\mathbf{x}) \mathcal{R}(u^{\delta}) dx = 0 \tag{4}$$

Equation 4 will lead to a system which solution yields the coefficients $\hat{u}_j$, which are used to obtain the desired solution from Eq. 3. When solving time-dependent PDEs, the Galerkin method provides an ordinary differential equation for $d\hat{\mathbf{u}}/dt$, which is further marched in time to obtain the desired solution at any time t. For the interested reader, more details about the CG method can be found in Karniadakis and Sherwin (2005).

2.2 Computational domain, mesh and setup parameters

The mixing layer simulated here is defined by the initial Reynolds number (see Eq. 5) based on the velocity difference, $\Delta U = 1$, initial momentum thickness, $\theta_0 = 1$, and kinematic viscosity, ν. The momentum thickness is given by:

$$Re_{\theta_0} = \frac{\Delta U \, \theta_0}{\nu} \tag{5}$$

$$\theta = \int_{-\infty}^{\infty} \frac{u(y) - U_1}{U_2 - U_1} \left(1 - \frac{u(y) - U_1}{U_2 - U_1}\right) dy \tag{6}$$

Where $u(y)$ is the mean stream-wise velocity, U_1 and U_2 are the slow and fast free-stream velocities respectively. Here, U_1 is equal to 0,5 and U_2 is equal to 1,5. The kinematic viscosity is manually adjusted to provide a $Re_{\theta_0} = 1000$.

The 2D computational domain is defined by a bounding box of 600 θ_0 height and 700 θ_0 long, where the system origin is located at the half of the inlet. The mesh was created with unstructured triangular elements, where element size parameters were defined for the far and inner regions from/of the mixing layer, being (hmax, hmix, hmin) = (20 θ_0; 2 θ_0; $0,3\ \theta_0$). This procedure led to a mesh with 105518 elements.

The boundary conditions were defined as follows: a velocity profile was defined at the inlet in order to obtain the desired initial momentum thickness. This profile is given in Eq. 7, where the value of a is $0.5/\theta_0$. Note that the fast free-stream velocity is located at the lower inlet. Far-field boundary conditions were defined at the upper and lower boundaries and a zero relative pressure condition was defined at the outlet. The mesh and boundary condition are shown in Fig. 3.

Finally, the simulations were started with an initial condition equal to the velocity profile. Additional comments about the initial condition and boundary condition at the inlet are given below.

$$u = 1 - \frac{1}{2}\Delta U \tanh(ay) \tag{7}$$

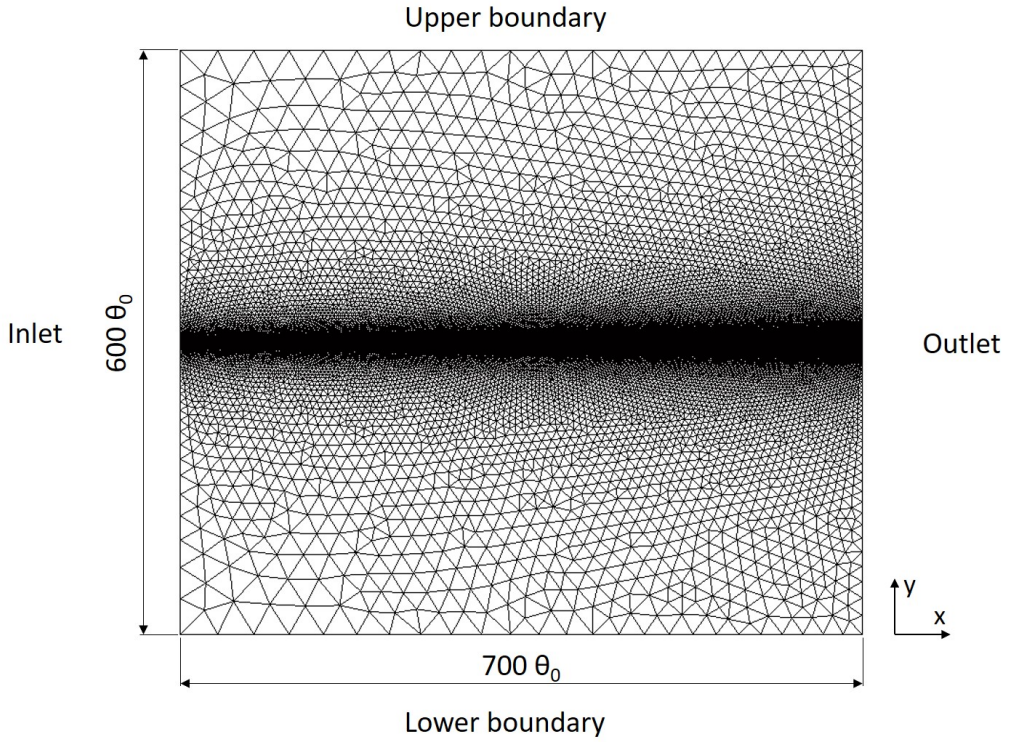

Figure 3: Mesh and boundary conditions.

No special treatment was given to trigger transition to turbulence, however previous attempts - not described here - have shown that introducing small magnitudes into the *u* and *b* velocity components contribute to anticipate the transition both in time and space. Also, previous analyses have shown that *w* component behaves likely as a conserved-scalar (marker field) in the adopted approach, which is described below. Therefore, the following values were setup to the *w*-velocity component in the initial conditions: -1 for y > 0 and +1 for y $\leq$ 0. This same values of *w* were added as boundary conditions at the inlet and at the same cross-stream positions. The *u*-velocity profile setup as initial and boundary condition is depicted in Fig. 4 for clarification. The simulation was run until $t = 1500$ with an implicit-explicit (IMEX) time-stepping scheme of second order and a non-dimensional time step equal to 4e-3. A Quasi-3D approach (2.5D) was also applied to extend the 2D domain to a pseudo-3D problem by specifying an harmonic expansion in the third direction (z-axis in this case). The length of the harmonic expansion was set to 0,01 with a number of quadrature points (or number of discretized 2D planes) equal to 2. This small discretization in the z-axis is the reason for the 2D behavior of the simulations. If one takes the momentum equation in the z-axis (see Eq. 2) and set the derivatives in the z-direction ($\partial/\partial z$) to zero, then the equation becomes a convection-diffusion equation as shown in Eq. 8. Finally, a forth-order spatial discretization with a spectral/hp dealiasing (Kirby and Sherwin, 2006) and GJP stbilization techniques were used to simulate the mixing layer flow in the open-source software Nektar++ (Nektar++, 2014; Cantwell *et al.*, 2015).

$$\rho\left(\frac{\partial w}{\partial t} + u\frac{\partial w}{\partial x} + v\frac{\partial w}{\partial y}\right) = \mu\left(\frac{\partial^2 w}{\partial x^2} + \frac{\partial^2 w}{\partial y^2}\right) \tag{8}$$

2.3 Mixing layer description

A mixing layer has a dominant direction of the flow, x - the stream-wise direction, a cross-stream direction, y, and is statistically independent of the span-wise coordinate, z. In addition, the two inlet velocities characterize a non-dimensional velocity (U_1/U_2) and two characteristic velocities: the convection velocity $\left(U_c \equiv \frac{1}{2}(U_1 + U_2)\right)$ and the velocity difference, ΔU, previously presented.

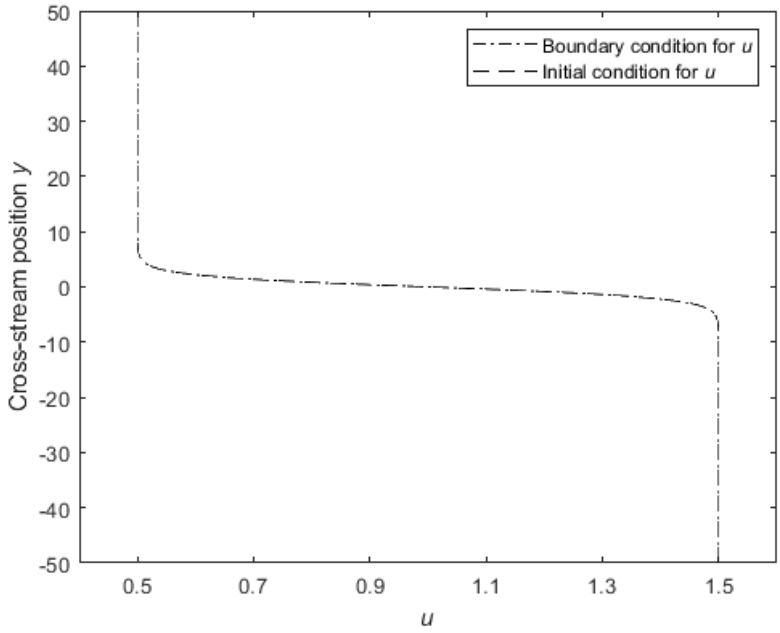

Figure 4: *u*-velocity profile defined at the inlet and as initial condition.

One can define a characteristic width of the flow based on the mean velocity profile $\langle U(x, y, z)\rangle$. For that, it's first introduced a cross-stream location $y_\alpha(x)$ for $0 < \alpha < 1$ so that:

$$\langle U(x, y_\alpha(x), 0)\rangle = U_1 + \alpha(U_2 - U_1) \tag{9}$$

Then the characteristic width, $\delta(x)$, is defined as:

$$\delta(x) = y_{0,9}(x) - y_{0,1}(x) \tag{10}$$

Under specific scaled coordinate and velocity, a mixing layer has a self similar behavior for high-enough Re. Also, it has be shown that a mixing layer posses a constant spreading rate ($S = d\delta/dx$) between approximately 0,06 and 0,11, which will depend in part to the state of the flow at the inlet. For more details, please refer to Pope (2000). The Re of a mixing layer can be also defined by its characteristic width as shown in Eq. 11. So, as the characteristic velocity difference is constant and the characteristic width varies linearly with the stream-wise direction, the Reynolds number also increases linearly with x as previously stated in Sec. 1.

$$Re(x) = \frac{\Delta U\, \delta(x)}{\nu} \tag{11}$$

3. RESULTS AND DISCUSSION

This section presents the current results of the 2D mixing layer analysis for capturing the mixing transition with a turbulence model-free under-resolved simulation.

Figure 5 shows the spatial development of the mixing layer for different time-snapshots. One can see that the instabilities start to grow around t = 250 and the initial vortices are carried outside the domain just after t = 750. From t = 1000 onwards, the mixing layer is totally developed and the flow is statistically stationary as shown in Fig. 6. Here, the time-average of the accumulated characteristic width is shown for a *x*-coordinate position of 550 and for different time window values starting from t = 1000. From the time window of 400, i.e. the time-average between t = 1000 and t = 1400, its possible to observe that the statistical quantity (averaged characteristic width) has converged and we take the value of $\delta_{t\,=\,500}$ = 31.4 as the local characteristic width of the mixing layer, which leads to a local *Re* of $3,14 \times 10^4$. As for the *w*-velocity component (see Fig. 7), one can see that its mixture follows the development of the mixing layer, which is highlighted in Fig. 5. Again, it is possible to observe that the initial vortices leave the domain after t = 750. This is directly observed by the fact that the great perturbation seen in Figs. 5c and 7c is not seen anymore in times greater than 1000. Also, if we consider the convective characteristic velocity of the studied flow (U_c = 0,75) and the distance from the first vortices in Fig. 7b to the outlet, which is around 300, a time of 400 would be required for the exit of all those vortices.

Two magnified views of the mixing layer for t = 1000 are presented in Fig. 8. One can see that the *w*-velocity field is quite simple in the image of the left. At this location ($360 \leq x \leq 480$), the Re is not high enough and the fluid basically

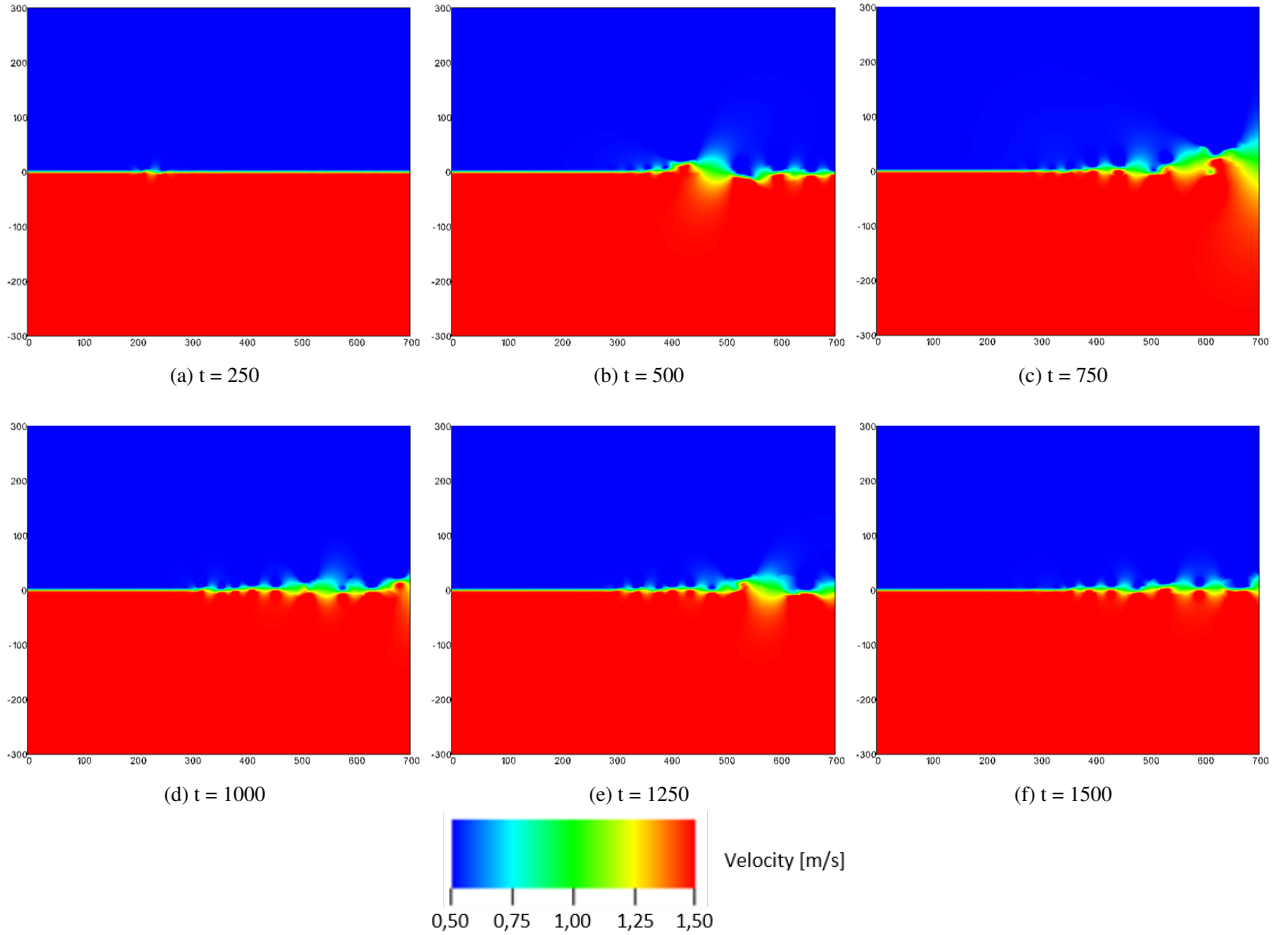

Figure 5: Development of *u*-velocity field of the mixing layer for different time-snapshots.

alternates between the high-speed fluid (U_2) to the low-speed fluid (U_1), showing that there is a little mixing between the fluids, being specifically at the interface regions. As for the image on the right, there are regions with more mixing than the last image, which are shown by the broader brand of colors between the two layers, resulting in a smoother gradient of the *w*-velocity. These results seem to be in accordance with the study of Koochesfahani and Dimotakis (1986). They researched the behavior of mixing layers under different configurations. For comparison purposes, Fig. 9 presents a space-time slice of the concentration field of each fluid at a fixed downstream location. In this figure, the color red represents the low-speed fluid, whereas the blue represents the high-speed fluid. In the left image, which shows the mixing layer at a $Re \approx 1,75 \times 10^3$, a mixing between the layers is almost not seen. On the other hand, the right image shows big regions with intermediate concentration of the fluids, showing that the mixing had a great increase from $Re \approx 1,75 \times 10^3$ to $Re \approx 2,30 \times 10^4$ in a similarly way as observed in this study. However, Fig. 8 does not show a mean dominated mixture as in Fig. 9. Probably, this is because they studied a real 3D mixing layer, which also suggest that a more similar behavior may be found in a higher *Re* number, even though the *Re* range of the observed region is already above the *Re* range of Koochesfahani and Dimotakis (1986) study.

4. CONCLUSIONS AND FUTURE STUDIES

This article has initially approached the mixing transition phenomenon in a mixing layer using a turbulence model-free under-resolved simulation (uDNS or also known as iLES). Specifically, the spectral/*hp* Continuous Galerkin scheme was utilized in this analysis.

The flow was studied using a Quasi-3D approach (2.5D) to extend the 2D domain to a 3D problem by specifying an harmonic expansion. Also, the simulations were run in the open-source Nektar++ software, which supports the high-order discretization methods (CG and DG).

This initial study was able to show the spatial development of the mixing layer throughout the domain, where the turbulent regions are highlighted by the velocity fluctuations and the mixture. Also, the *w*-velocity component contour field, acting here as a scalar field due to the thin domain (z-direction), satisfactorily showed, in a qualitative way, the

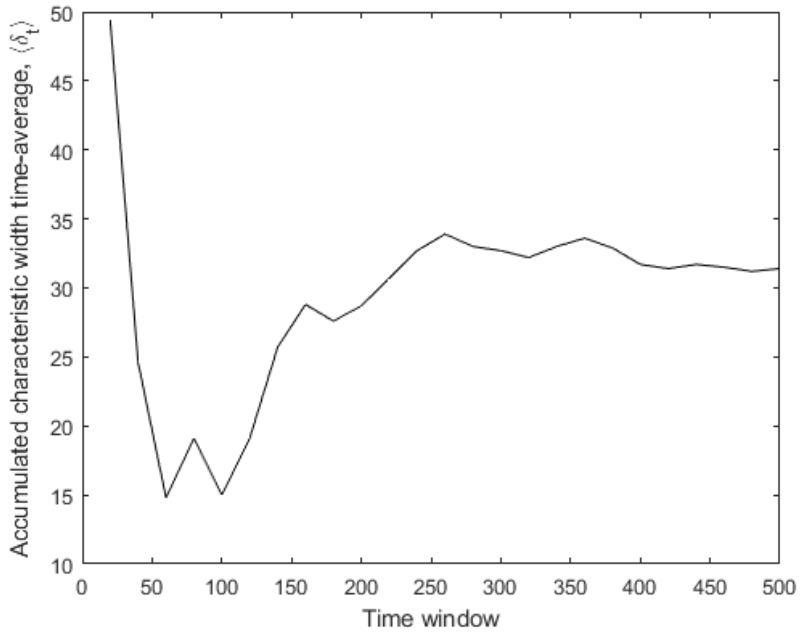

Figure 6: Accumulative time-average of the mixing layer's characteristic width at a x-coordinate position of 550. Time averages start from t = 1000.

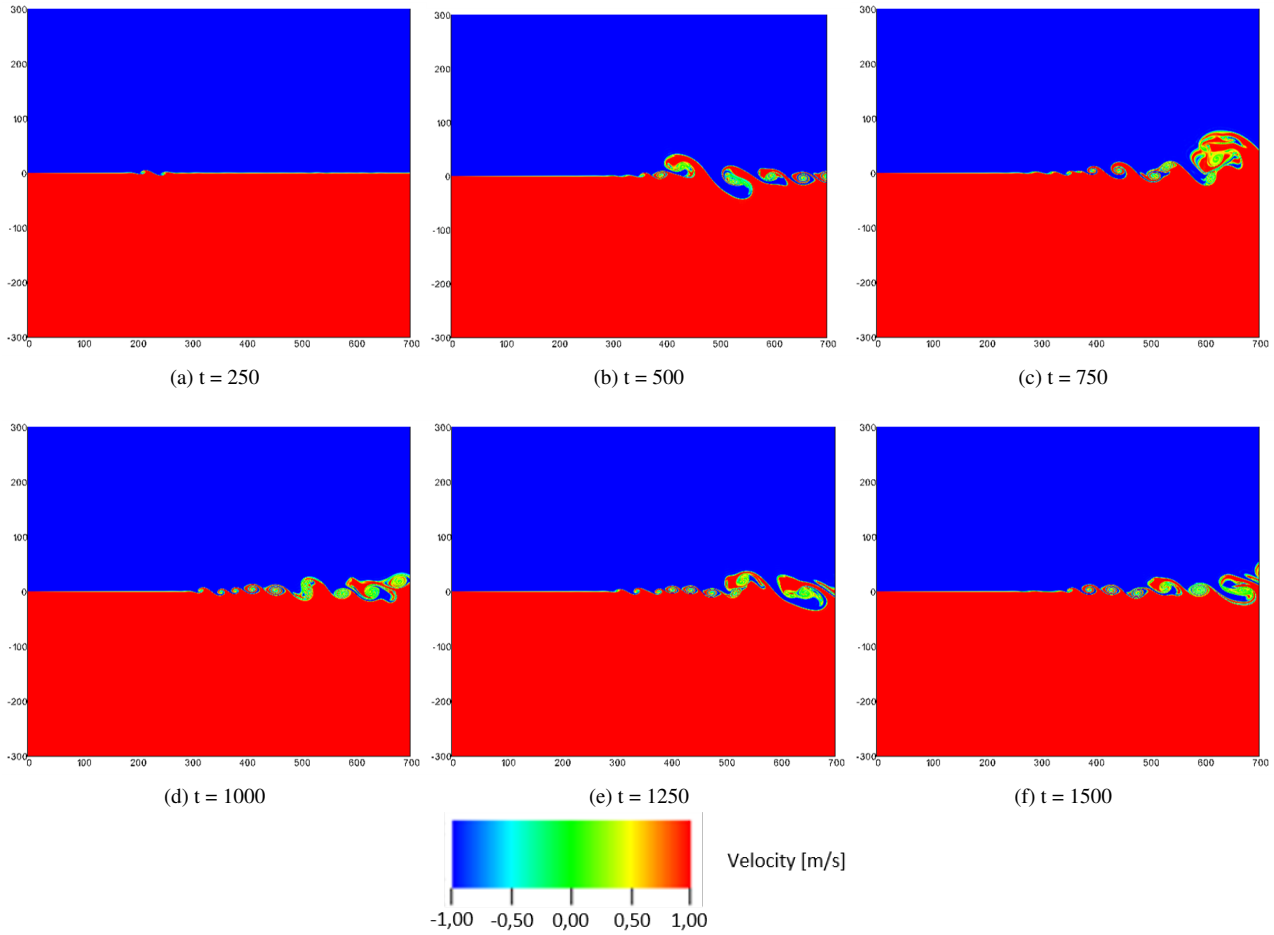

Figure 7: Development of *w*-velocity field of the mixing layer for different time-snapshots.

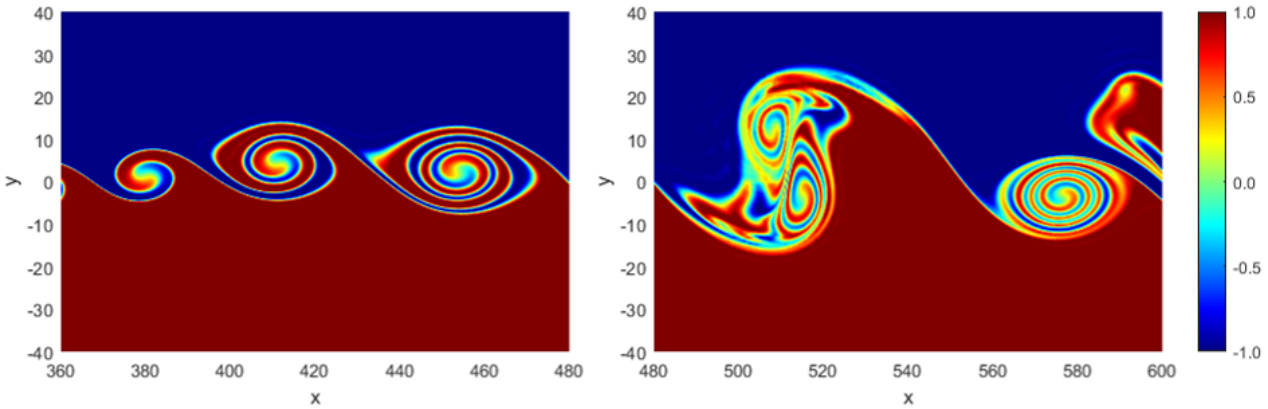

Figure 8: w-velocity field of the mixing layer for t = 1000 and two different spatial-window locations.

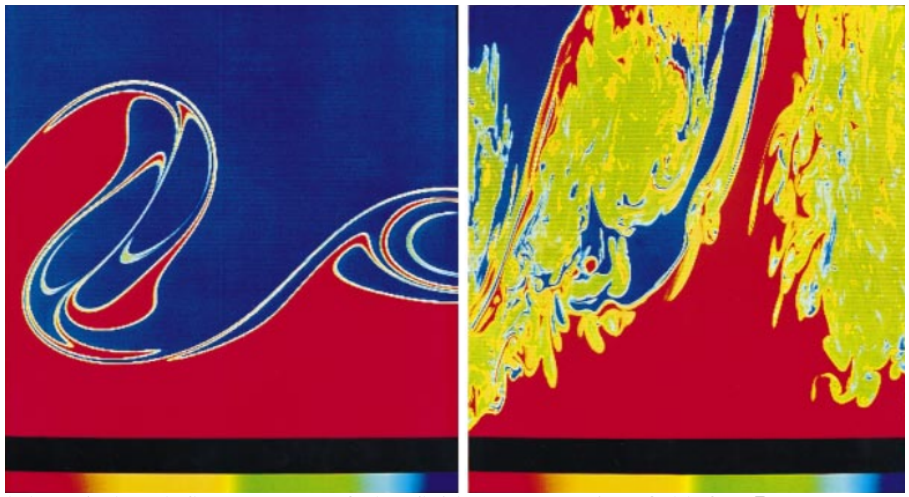

Figure 9: Digital laser-induced fluorescence of the fluids concentration field for $Re \approx 1,75 \times 10^3$ (left) and $Re \approx 2,30 \times 10^4$ (right). Reproduced from Koochesfahani and Dimotakis (1986).

mixing occurring along the mixing layer. Also, from a specific stream-wise position, it was possible to observe a more mixed region, where the velocity gradient was not steep anymore. Comparing with the literature, we believe that this is evidence of the mixing transition phenomenon.

However, this research finds itself in an initial part and further studies are required. For instance, in order to quantitatively describe the mixing transition, frequency spectrum are to be determined in the mixing regions, where high frequencies are expected to dominate in regions before the mixing transition, whereas a better distributed spectrum would be found in the mixing transition region onward. Finally, 2.5D simulation with a higher number of expansion planes and also 3D simulations will be run in the future.

5. ACKNOWLEDGEMENTS

The authors acknowledge support from CAPES (Coordenação de Aperfeiçoamento de Pessoal de Nível Superior - Brasil - Finance Code 001) and CNPq (Conselho Nacional de Desenvolvimento Científico e Tecnológico - Brasil), specially the first author who is a CNPq scholarship holder (Process number 141515/2021-0). Also, the authors acknowledge the members of LASCA laboratory group (ITA) and FAPESP (Process number 2020/10910-8).

6. REFERENCES

Brown, G.L. and Roshko, A., 1974. "On density effects and large structure in turbulent mixing layers". *Journal of Fluid Mechanics*, Vol. 64, No. 4, p. 775–816. doi:10.1017/S002211207400190X.

Cantwell, C., Moxey, D., Comerford, A., Bolis, A., Rocco, G., Mengaldo, G., De Grazia, D., Yakovlev, S., Lombard, J.E., Ekelschot, D., Jordi, B., Xu, H., Mohamied, Y., Eskilsson, C., Nelson, B., Vos, P., Biotto, C., Kirby, R. and Sherwin, S., 2015. "Nektar++: An open-source spectral/hp element framework". *Computer Physics Communications*, Vol. 192, pp. 205–219. doi:https://doi.org/10.1016/j.cpc.2015.02.008.

Dimotakis, P.E., 2000. "The mixing transition in turbulent flows". *Journal of Fluid Mechanics*, Vol. 409, p. 69–98.

doi:10.1017/S0022112099007946.

Karniadakis, G.E. and Sherwin, S., 2005. *Spectral/hp element methods for computational fluid dynamics*. Oxford University Press on Demand, 2nd edition.

Kirby, R.M. and Sherwin, S.J., 2006. "Stabilisation of spectral/hp element methods through spectral vanishing viscosity: Application to fluid mechanics modelling". *Computer Methods in Applied Mechanics and Engineering*, Vol. 195, No. 23, pp. 3128–3144. doi:https://doi.org/10.1016/j.cma.2004.09.019. Incompressible CFD.

Koochesfahani, M.M. and Dimotakis, P.E., 1986. "Mixing and chemical reactions in a turbulent liquid mixing layer". *Journal of Fluid Mechanics*, Vol. 170, p. 83–112. doi:10.1017/S0022112086000812.

Nektar++, 2014. *Nektar++: Spectral/hp Element Framework*. Department of Aeronautics, Imperial College London and Scientific Computing and Imaging Institute, University of Utah. URL `https://www.nektar.info/getting-started/documentation/`.

Papamoschou, D. and Gharib, M., 2020. "Anatol roshko, 1923–2017". *Annual Review of Fluid Mechanics*, Vol. 52, No. 1, pp. 1–18. doi:10.1146/annurev-fluid-010719-060122.

Pope, S.B., 2000. *Turbulent Flows*. Cambridge University Press. doi:10.1017/CBO9780511840531.

Silveira Neto, A., 2020. *Escoamentos Turbulentos: Análise Física e Modelagem Teórica*. Composer, Universidade Federal de Uberlândia.

7. RESPONSIBILITY NOTICE

The authors are the only responsible for the printed material included in this paper.